

Superclusters with thermal SZ effect surveys

Antonaldo Diaferio,¹ Adi Nusser,² Naoki Yoshida,³ Rashid A. Sunyaev^{4,5}

¹*Dipartimento di Fisica Generale “Amedeo Avogadro”, Università degli Studi di Torino, Italy*

²*Department of Physics, Technion-Israel Institute of Technology, Technion City, Haifa, Israel*

³*Harvard-Smithsonian Center for Astrophysics, Cambridge, MA, USA*

⁴*Max-Planck Institut für Astrophysik, Garching, Germany*

⁵*Space Research Institute (IKI), Russian Academy of Sciences, Moscow, Russia*

10 November 2018

ABSTRACT

We use a simple analytic model to compute the angular correlation function of clusters identified in upcoming thermal SZ effect surveys. We then compute the expected fraction of close pairs of clusters on the sky that are also close along the line of sight. We show how the expected number of cluster pairs as a function of redshift is sensitive to the assumed biasing relation between the cluster and the mass distribution. We find that, in a Λ CDM model, the fraction of physically associated pairs is 70% for angular separations smaller than 20 arcmin and clusters with specific flux difference larger than 200 mJy at 143 GHz. The agreement of our analytic results with the Hubble volume N -body simulations is satisfactory. These results quantify the feasibility of using SZ surveys to compile catalogues of superclusters at any redshifts.

Key words: large scale structure of Universe – galaxies: clusters: general – cosmology: miscellaneous – methods: analytical

1 INTRODUCTION

Superclusters are regions with average mass overdensities larger than a few, on scales larger than a few megaparsecs; their cluster members show indications of intense dynamical activity and provide evidence that structures form hierarchically on supercluster scales (e.g. Bardelli, Zucca & Baldi 2001; Rines et al. 2001; Plionis & Basilakos 2002).

Analyses of catalogues of superclusters in the local Universe (e.g. Bahcall & Soneira 1984; West 1989; Zucca et al. 1993; Einasto et al. 2001), beyond the local supercluster (Oort 1983), have focused on their shapes and their large scale distribution (Kerscher 1998). Shape statistics have been used for discriminating among the cosmological models (Basilakos, Plionis & Rowan-Robinson 2001; Kolokotronis, Plionis & Basilakos 2002), whereas the total mass of superclusters can be used to estimate the density parameter Ω_0 from the mass-to-light ratio on large scales (Small et al. 1998). At high redshift, superclusters, when they exist (Postman et al. 2002), are difficult to identify, although preferred directions of radio emission from distant quasars and radio galaxies (West 1991) or unusual X-ray morphologies (Hashimoto et al. 2002) can provide evidence of their existence at $z \gtrsim 1$.

The peculiar velocities of clusters are enhanced in superclusters by non-linear effects (Zucca et al. 1993; Bahcall, Gramann & Cen 1994). Colberg et al. (2000a) have indeed shown that the peculiar velocity of dark matter halos with massive neighbours in N -body simulations is $\sim 40 - 50\%$ larger than predicted by linear theory. In fact, linear theory predicts that the evolution of the peculiar velocities is independent of the local density, whereas Sheth & Diaferio (2001) have shown that, in N -body simulations, evolved peculiar velocities of halos with the same mass are larger (smaller) in high (low) density regions. Moreover, the high velocity tail of the cluster peculiar velocity distribution can be a sensitive discriminator of cosmological models (Bahcall et al. 1994; Peel & Knox 2002). In N -body simulations of representative volumes of the Universe, high density regions of a few megaparsec size contain two or more massive clusters; these superclusters can be easily spot in thermal Sunyaev & Zel’dovich (1980; SZ) effect surveys as nearby CMB temperature decrements in the Rayleigh-Jeans limit and are the favorite regions for searches of enhanced kinematic SZ effect (Diaferio, Sunyaev & Nusser 2000). Confusion caused by primary Cosmic Microwave Background (CMB) anisotropies, thermal SZ and instrumental noise, complicates the estimation of cluster peculiar velocities from measurements of the kinematic effect (Aghanim, Gorski & Puget 2001). The kinematic SZ

effect is difficult to detect directly; it is roughly an order of magnitude smaller than the thermal effect. One may proceed by looking for kinematic fluctuations in clusters selected according to thermal SZ measurements. However the most massive clusters that are responsible for the largest thermal fluctuations do not necessarily have the largest peculiar velocities.

The thermal SZ effect, being independent of redshift, is the optimal tool for detecting clusters at high redshifts (Carlstrom 2002). Several SZ surveys will produce catalogues of thousands clusters at any redshift in the next few years, e.g. SPT (Carlstrom 2002), AMI (Kneissl et al. 2001), AMiBA (Lo et al. 2002), to mention a few.

Clusters are not randomly distributed on the sky: their angular correlation function mirrors the clustering evolution of mass. The angular correlation function of SZ clusters was first computed by Cole & Kaiser (1988) who were interested in the non-Gaussianity of CMB temperature fluctuations caused by galaxy clusters. Komatsu & Kitayama (1999) show that the correlation in the cluster distribution enhances by $\sim 20 - 30\%$ the Poisson contribution to the CMB angular power spectrum at degree angular scales. Moscardini et al. (2002) compute the correlation function on the light-cone of clusters detectable by the Planck surveyor satellite and show that the correlation length of these SZ selected clusters is more sensitive to the physical properties of the ICM than to the cosmological parameters.

In this paper we use a simple analytic model to compute the angular correlation function and the fraction of pairs that are close along the line of sight as well as on the sky. Our result shows that for viable cosmological models, this fraction is substantial. Therefore if we define superclusters as regions containing two or more close clusters, this result motivates the use of thermal SZ cluster surveys to identify superclusters at any redshift. We also compute the expected number count of cluster *pairs* within a given separation as a function of redshift. Unlike the number count of individual clusters, the pair number count is sensitive to the assumed form of the bias function between the cluster and the mass distribution.

In section 2 we outline the basic equations; in section 3 we compute the expected number of clusters per solid angle in flux limited thermal SZ surveys, their angular correlation function and the number of physically associated pairs; we then apply our model to a full sky survey like the Planck surveyor. In section 3.5 we show how the fraction of physically associated pairs depend on the assumed biasing relation. We conclude in section 4.

2 BASIC EQUATIONS AND DEFINITIONS

The interaction between the CMB radiation field and the hot cloud of electrons in the ICM plasma changes the specific intensity of the radiation. The difference in the specific intensity ΔI_ν at frequency ν is (SZ)

$$\Delta I_\nu = i_0 g(x) y = i_0 g(x) \frac{k\sigma_T}{m_e c^2} \int n_e(r) T_e(r) dl, \quad (1)$$

where $i_0 = 2(kT)^3/(h_P c)^2$, k is the Boltzmann constant, $T = 2.725$ K the present day CMB temperature (Mather et al. 1999), h_P the Planck constant, c the speed of light, σ_T the Thomson cross section, m_e the electron mass, $x = h_P \nu/kT$,

$$g(x) = \frac{x^4 e^x}{(e^x - 1)^2} \left(x \frac{e^x + 1}{e^x - 1} - 4 \right), \quad (2)$$

and n_e and T_e the electron number density and temperature, respectively. The integral is over the line of sight l , $r^2 = w^2 + l^2$, where w is the separation from the cluster center projected onto the sky, and we assume that the cluster is spherically symmetric. Here, we neglect the contribution of the kinematic effect. Let

$$\langle T_e \rangle_n = \frac{\int n_e(r) T_e(r) dV}{\int n_e(r) dV} \sim \frac{R_p^2}{N_e^{tot}} \int n_e(r) T_e(r) dl \quad (3)$$

be the electron density weighted mean temperature, where R_p is the projected proper size of the cluster and N_e^{tot} the total number of electrons in the cluster. The variation of the CMB specific flux after passing through the cluster is

$$F_\nu = \int \Delta I_\nu d\Omega \approx \Delta I_\nu \Delta\Omega = i_0 g(x) \frac{k\sigma_T}{m_e c^2} \frac{f_g}{\mu_e m_p} \frac{1}{d_A^2(z)} \langle T_e \rangle_n M \quad (4)$$

where we have assumed an effective solid angle $\Delta\Omega = R_p^2/d_A^2(z)$, $d_A(z)$ is the angular diameter distance, $N_e^{tot} = M f_g / \mu_e m_p$, M is the total mass of the cluster, f_g the gas fraction, μ_e the mean molecular weight per electron, and m_p the proton mass. Hereafter, we adopt $f_g = 0.06 h^{-3/2}$, which has been derived from a sample of 36 X-ray luminous clusters with redshift in the range 0.05 – 0.44 (Ettori & Fabian 1999); here, for simplicity, we neglect (1) the observed variation, up to $\sim 50\%$, of f_g between clusters, and (2) the observed dependence of f_g on redshift; note that this dependence is weaker in low-density Universes than in high-density Universes. Assuming a fully ionized ICM of hydrogen and helium with a helium mass fraction $Y = 0.24$, the mean molecular weight per electron is $\mu_e = (1 - Y/2)^{-1} = 1.136$.

X-ray observations indicate that the ICM temperature is roughly proportional to $M^{2/3}$ where M is the virial mass of the cluster (e.g. Finoguenov, Reiprich & Böhringer 2001; Allen, Schmidt & Fabian 2001), in agreement with arguments based on the virial theorem. Hydrodynamical simulations of cluster formation give similar slope for the $T - M$ relation, but the

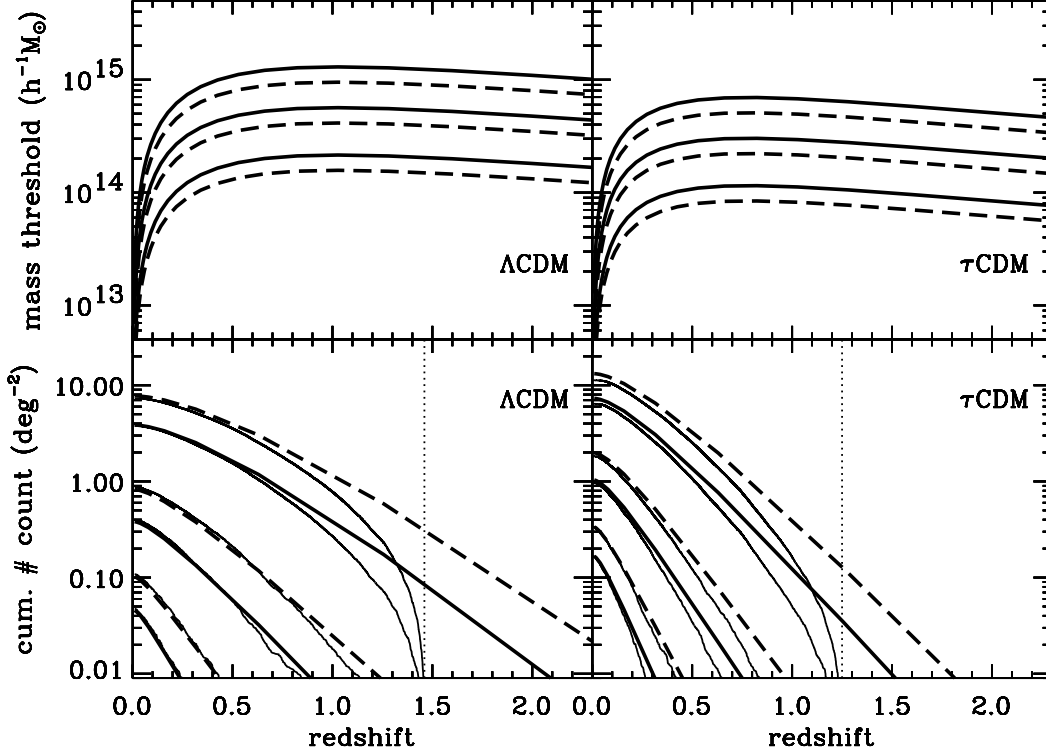


Figure 1. Upper panels: mass threshold corresponding to $F_{\nu}^{\min} = 200, 50, 10$ mJy (top to bottom) for $\nu = 143$ GHz (solid) and $\nu = 353$ GHz (dashed lines). Lower panels: redshift cumulative cluster number counts corresponding to $F_{\nu}^{\min} = 10, 50, 200$ mJy (top to bottom). Bold lines are the expected distribution (equation 8); thin lines are the actual number from the Hubble volume simulations. Dotted lines indicate the redshift limit of the lightcone outputs.

temperatures are higher by a factor of two or so (e.g. Mathiesen & Evrard 2001). Simulations might miss some important ingredient of the ICM physics; thus, we adopt a $T - M$ relation in agreement with X-ray observations, i.e.,

$$\langle T_e \rangle_n = 0.43 [\Delta_c(z) H^2(z) / H_0^2]^{1/3} \left(\frac{M}{10^{14} h^{-1} M_{\odot}} \right)^{2/3} \text{ keV}, \quad (5)$$

where h is the present day Hubble constant H_0 in units of $100 \text{ km s}^{-1} \text{ Mpc}^{-1}$, $H^2(z) = H_0^2 [\Omega_0(1+z)^3 + (1-\Omega_0-\Lambda_0)(1+z)^2 + \Lambda_0]$, and $\Delta_c(z)$ is the mass density of the cluster, which has just collapsed at redshift z , in units of the critical density at that redshift (Bryan & Norman 1998). Note that here we assume valid the simple top-hat collapse model, although Voit (2000) shows that this assumption may be too simplistic when used to derive the evolution of the mass-temperature relation. We also assume that the X-ray temperature equals the electron density mean weighted temperature $\langle T_e \rangle_n$.

The specific flux variation becomes

$$F_{\nu} = 9.33 \times 10^4 \left(\frac{T}{\text{K}} \right)^3 g(x) \frac{h f_g}{\mu_e} \left(\frac{h^{-1} \text{Mpc}}{d_A(z)} \right)^2 [\Delta_c(z) H^2(z) / H_0^2]^{1/3} \left(\frac{M}{10^{14} h^{-1} M_{\odot}} \right)^{5/3} \text{ mJy}. \quad (6)$$

SZ surveys will be able to detect only specific flux differences larger than a threshold F_{ν}^{\min} . This constraint translates into a mass threshold M_{th} below which clusters remain undetected:

$$\frac{M_{\text{th}}(z, F_{\nu}^{\min})}{10^{14} h^{-1} M_{\odot}} = 1.04 \times 10^{-3} \left(\frac{\mu_e}{h f_g} \right)^{3/5} \left(\frac{T}{\text{K}} \right)^{-9/5} g^{-3/5}(x) \left(\frac{d_A(z)}{h^{-1} \text{Mpc}} \right)^{6/5} [\Delta_c(z) H^2(z) / H_0^2]^{-1/5} \left(\frac{F_{\nu}^{\min}}{\text{mJy}} \right)^{3/5}. \quad (7)$$

The top panels in figure 1 show $M_{\text{th}}(z, F_{\nu}^{\min})$ for two frequencies measurable by the High Frequency Instrument (HFI) of the Planck surveyor satellite in two cosmological models (see section 3 for details on the models). Except for an initial rapid increase, M_{th} varies slowly with redshift. This feature effectively makes a flux-limited SZ survey a mass-limited survey (Bartlett & Silk 1994).

3 STATISTICS OF THE CLUSTER DISTRIBUTION

In this section, we compute the redshift distribution of individual clusters, the cluster angular correlation function $w(\theta)$, and the redshift distribution of physically associated cluster pairs.

We compare our analytic calculations with the *lightcone* outputs of the two Hubble volume simulations (Evrard et al. 2002; Yoshida et al. 2001). These two simulations correspond to a Λ CDM and a τ CDM cosmology with $(\Omega_0, \Lambda_0, h, \sigma_8) = (0.3, 0.7, 0.7, 0.9)$ and $(1, 0, 0.5, 0.6)$, respectively. For both models, the power spectrum shape parameter is $\Gamma = 0.21$ (Frenk et al. 2000; see Evrard et al. 2002 for further details). Using the lightcone outputs has the advantage of simulating a more realistic observation of a patch of the sky when compared to the usual technique of stacking simulation boxes at different redshifts (e.g. Scaramella, Cen & Ostriker 1993; da Silva et al. 2000; Seljak, Burwell & Pen 2000; Springel, White & Hernquist 2001; Zhang, Pen & Wang 2002). Dark matter halos in the N -body simulations have been identified with a spherical overdensity technique. We assume that these halos do correspond to galaxy clusters in the appropriate mass range, although comparisons with the APM cluster catalogue show slightly different clustering properties (Colberg et al. 2000b).

3.1 Number count of individual clusters

The number count η per unit solid angle of clusters as microwave sources, as compared to X-ray sources, was first computed by Korolev, Sunyaev & Yakubsev (1986); many authors, which were interested in different aspects of η , have computed it ever since (see e.g. Bartlett 2001 and references therein). The number count η enters the calculation of the angular correlation function (section 3.2). It is sensitive to the properties of the ICM (Holder & Carlstrom 2001; Benson et al. 2002) and to the cosmological parameters (Barbosa et al. 1996; Kneissl et al. 2001; Haiman, Mohr & Holder 2001; Holder, Haiman & Mohr 2001; Benson, Reichardt & Kamionkowski 2002). The number count also depends on the parameters of the survey, namely its sensitivity (or its flux limit F_ν^{lim}) and its angular resolution. The cumulative number count of clusters, at redshift greater than z , detected per unit solid angle is

$$\eta(z, F_\nu^{\text{lim}})d\Omega = d\Omega c \int_z^\infty \frac{d^2(z_1)}{H(z_1)} dz_1 \int_{M_{\text{th}}(z_1, F_\nu^{\text{lim}})}^\infty \frac{dn(M, z_1)}{dM} dM \quad (8)$$

where $d(z) = (1+z)d_A(z)$ is the distance measure, and $dn(M, z)/dM$ is the comoving number density of clusters with mass in the range $(M, M+dM)$ at redshift z . We have assumed that the detector is able to measure the total specific flux difference F_ν of each cluster. When the angular resolution of the survey is included in the analysis, the cluster number count can drop significantly (Bartlett 2000).

In the Hubble volume simulations, the dark matter halo mass function is well fitted by the formula (Jenkins et al. 2001)

$$\frac{dn_J(M, z)}{dM} dM = \frac{A\langle\rho\rangle}{M} \alpha_{\text{eff}}(M) \exp[-|\ln \sigma^{-1}(M) + B|^\epsilon] dM \quad (9)$$

where $(A, B, \epsilon) = (0.22, 0.73, 3.86)$ and $(0.27, 0.65, 3.77)$ for the Λ CDM and τ CDM model, respectively, $\langle\rho\rangle$ is the comoving mean density, $\alpha_{\text{eff}} = d \ln \sigma^{-1}(M)/d \ln M$,

$$\ln \sigma^{-1}(M) = -\ln \sigma_{15} + a \ln M + b(\ln M)^2 \quad (10)$$

and $(\sigma_{15}, a, b) = (0.578, 0.281, 0.0123)$ and $(0.527, 0.267, 0.0122)$ for the Λ CDM and τ CDM model, respectively.

The lower panels of figure 1 show the redshift cumulative cluster number count for the two models (thin lines) compared with the expectation of equation (8). We use the *NO* lightcone outputs of the Hubble volume simulations, which cover $\pi/2$ sr and have depth $z = 1.46$ (Λ CDM) and 1.25 (τ CDM), as indicated by the dotted lines. The disagreement at low F_ν^{lim} and at high redshift is mainly due to the mass resolution limit.

3.2 The angular correlation function

To compute $w(\theta)$, we need to know the three dimensional two-point correlation function $\xi(r_{12}, M_1, M_2, z_1, z_2)$ for clusters of mass M_1, M_2 at redshift z_1, z_2 and comoving separation r_{12} . When $z_1 = z_2 = z$, we can use the simple biasing scheme

$$\xi(r_{12}, M_1, M_2, z) = b_{\text{ST}}(M_1, z) b_{\text{ST}}(M_2, z) \xi_m(r_{12}, z) \quad (11)$$

where (Sheth & Tormen 1999)

$$b_{\text{ST}}(M, z) = 1 + \frac{a\nu^2 - 1}{\delta_c(z)} + \frac{2p}{\delta_c(z)[1 + (a\nu^2)^p]}, \quad (12)$$

$a = 0.707$, $p = 0.3$, $\nu = \delta_c(z)/\sigma(M, z)$, $\sigma(M, z)$ is the rms of the mass density field smoothed on scale $R = (3M/4\pi\langle\rho\rangle)^{1/3}$, $\langle\rho\rangle$ is the mean comoving mass density, and $\delta_c(z)$ is the linear overdensity extrapolated at redshift z for a spherical perturbation which has just collapsed (see Kitayama & Suto 1996 or Nakamura & Suto 1997 for handy fitting formulae to these quantities);

$\xi_m(r, z)$ is the correlation function of dark matter at redshift z . Equation (12) is strictly valid on large scales. Because we are interested in close pairs of clusters, we need to consider a scale dependent bias factor $b(r, M, z)$ (e. g. Yoshikawa et al. 2001). For clusters at different redshifts z_1 and z_2 , we can modify equation (11) to

$$\xi(r_{12}, M_1, M_2, z_1, z_2) = b(r_{12}, M_1, z_1)b(r_{12}, M_2, z_2)\xi_m(r_{12}, z_1) \quad (13)$$

where we break the symmetry in z_1 and z_2 by ‘‘sitting’’ on the cluster at z_1 . Equation (13) is consistent with equation (11), because clusters at different epochs z_1, z_2 are not correlated and $\xi(r_{12})$ goes to zero with increasing r_{12} quickly enough that $\xi(r_{12}) \neq 0$ only when $z_1 \sim z_2$. Alternative choices of the redshift at which ξ_m can be computed are discussed in Porciani (1997).

The comoving relative separation r_{12} in a space described by the Robertson-Walker metric is (Weinberg 1972, equation 14.2.7; Osmer 1981)

$$r_{12}^2(z_1, z_2, \theta) = d^2(z_1)G^2(z_1, z_2, \theta) + d^2(z_2) - 2d(z_1)d(z_2)G(z_1, z_2, \theta) \cos \theta \quad (14)$$

where θ is the angular separation of the two objects on the sky,

$$G(z_1, z_2, \theta) = \sqrt{1 - \kappa d^2(z_2)} + \left(1 - \sqrt{1 - \kappa d^2(z_1)}\right) \frac{d(z_2)}{d(z_1)} \cos \theta \quad (15)$$

and $\kappa = (H_0/c)^2(\Omega_0 + \Lambda_0 - 1)$. This equation is *not* symmetric in z_1 and z_2 for a non flat Universe ($\kappa \neq 0$). However, if we deal with distances smaller than the curvature radius of the Universe $1/\sqrt{|\kappa|}$, we have $1/\kappa \gg d^2(z_1)$ and $\gg d^2(z_2)$, and $G \sim 1$; this is the case of interest, because we expect $\xi(r_{12}) \sim 0$ at large separation. When $z_1 = z_2 = z$, $r_{12}^2 \sim 2d^2(1 - \cos \theta)$ for $\kappa d^2 \sim 0$, and we correctly recover $\theta = r_{12}/d(z)$ for small θ .

To compute the angular correlation function, we follow the classical argument that leads to Limber’s equation (Matarrese et al. 1997; Moscardini et al. 2000). Consider the probability of finding two clusters with different mass at different redshift

$$\zeta(r_{12}, M_1, M_2, z_1, z_2) dA_1 dA_2 = dV_1 dV_2 \frac{dn(M_1, z_1)}{dM_1} dM_1 \frac{dn(M_2, z_2)}{dM_2} dM_2 [1 + \xi(r_{12}, M_1, M_2, z_1, z_2)] \quad (16)$$

where $dA_i = dM_i dz_i d\Omega_i$, $d\Omega_i$ is the infinitesimal solid angle and $dV_i = cd^2(z_i) d\Omega_i dz_i / H(z_i)$ is the infinitesimal comoving volume. The probability of detecting two clusters at angular separation θ is proportional to

$$\begin{aligned} \psi(\theta) d\Omega_1 d\Omega_2 &= d\Omega_1 d\Omega_2 \int \zeta(r_{12}, M_1, M_2, z_1, z_2) dM_1 dM_2 dz_1 dz_2 \\ &= d\Omega_1 d\Omega_2 \eta_0^2(F_\nu^{\min}) [1 + w(\theta, F_\nu^{\min})] \end{aligned} \quad (17)$$

where $\eta_0(F_\nu^{\min}) = \eta(0, F_\nu^{\min})$, and

$$w(\theta, F_\nu^{\min}) = \frac{\Xi_0(\theta, F_\nu^{\min})}{\eta_0^2(F_\nu^{\min})} \quad (18)$$

is the angular correlation function we are seeking. All the clustering and biasing information is in the function

$$\begin{aligned} \Xi(z, \theta, F_\nu^{\min}) &= c^2 \int_{z_1}^{\infty} n(z_1, F_\nu^{\min}) \frac{d^2(z_1)}{H(z_1)} dz_1 \times \\ &\times \int_0^z n(z_2, F_\nu^{\min}) b_{\text{eff}}(r_{12}, z_1, F_\nu^{\min}) b_{\text{eff}}(r_{12}, z_2, F_\nu^{\min}) \xi_m(r_{12}, z_1) \frac{d^2(z_2)}{H(z_2)} dz_2 \end{aligned} \quad (19)$$

where

$$n(z, F_\nu^{\min}) = \int_{M_{\text{th}}(z, F_\nu^{\min})}^{\infty} \frac{dn(M, z)}{dM} dM \quad (20)$$

$$b_{\text{eff}}(r, z, F_\nu^{\min}) = n^{-1}(z, F_\nu^{\min}) \int_{M_{\text{th}}(z, F_\nu^{\min})}^{\infty} b(r, M, z) \frac{dn(M, z)}{dM} dM \quad (21)$$

and $\Xi_0(\theta, F_\nu^{\min}) = \Xi(0, \theta, F_\nu^{\min})$.

We use the fitting formula given by Peacock & Dodds (1996) to compute the correlation function of dark matter $\xi_m(r_{12}, z)$ in the non-linear regime. For the effective scale dependent bias factor b_{eff} we adopt the following fitting formula.

$$b_{\text{eff}}(r, z, F_\nu^{\min}) = b_{\text{ST,eff}}(z, F_\nu^{\min}) [1 + b_{\text{ST,eff}}(z, F_\nu^{\min}) \sigma(r, z)]^{0.35}, \quad (22)$$

where $\sigma(r, z)$ is the mass variance smoothed over the top-hat radius r , and

$$b_{\text{ST,eff}}(z, F_\nu^{\min}) = \frac{\int_{M_{\text{th}}(z, F_\nu^{\min})}^{\infty} b_{\text{ST}}(M, z) [dn_J(M, z)/dM] dM}{\int_{M_{\text{th}}(z, F_\nu^{\min})}^{\infty} [dn_J(M, z)/dM] dM}. \quad (23)$$

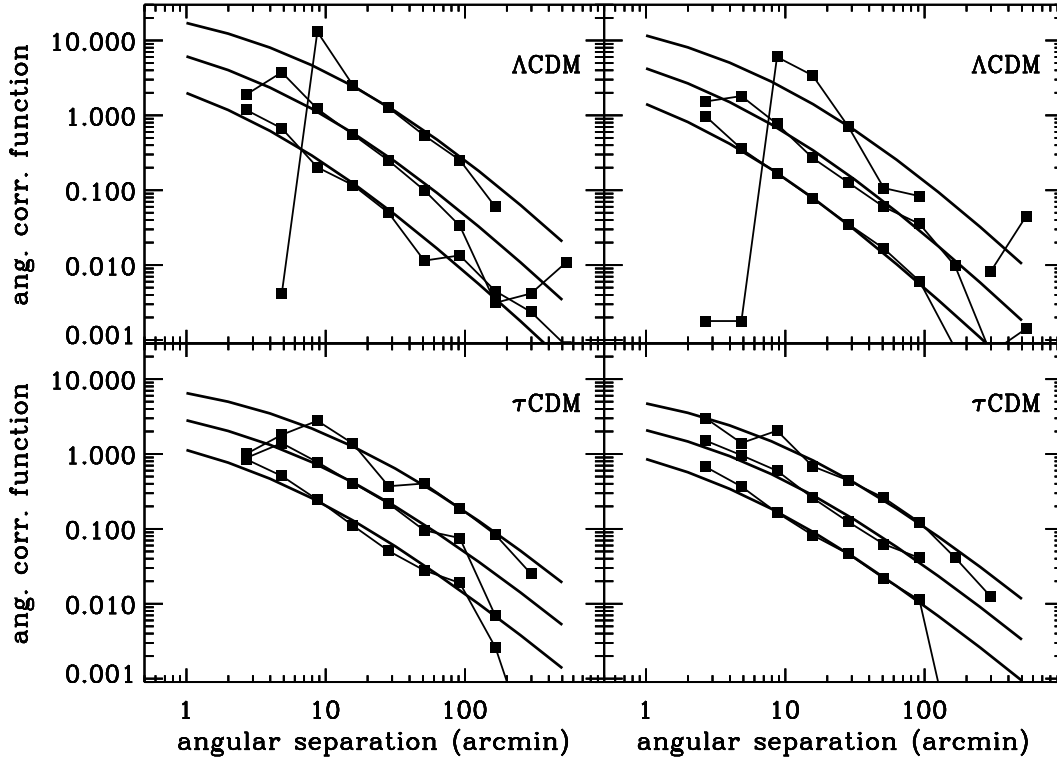


Figure 2. Angular correlation function of SZ clusters with $F_{\nu}^{\min} > 200, 50, 10$ mJy (top to bottom) for $\nu = 143$ GHz (left panels) and $\nu = 353$ GHz (right panels). Bold lines are the expected angular correlation function (equation 18); filled squares are the correlation function from the Hubble volume lightcones.

Figure 2 shows that this choice of the biasing relation yields an excellent agreement between the model and the angular correlation function derived from the pair count of SZ clusters in the N -body simulations. The functional form of the biasing relation (equation 22) was first suggested by Hamana et al. (2001), with a power 0.15 rather than 0.35. Hamana et al’s relation was only checked against the redshift zero output. When we compare the analytic modelling with the lightcone output, we include a broad redshift range, and the agreement shown in figure 2 indicates that a larger power seems more appropriate.

3.3 The number of physically associated cluster pairs

The fraction of pairs with angular separation smaller than θ whose cluster members have comoving separation along the line of sight smaller than r_{\max} is proportional to an expression similar to equation (19) where the integral over z_2 is limited to the interval set by r_{\max} . Because $\xi(r_{12}) \sim 0$ at large r_{12} , when r_{\max} is of order the cluster correlation length, we can estimate this fraction as

$$\varphi_0(< \theta) = \frac{\int_0^\theta w(\theta_1) \theta_1 d\theta_1}{\int_0^\theta [1 + w(\theta_1)] \theta_1 d\theta_1}. \quad (24)$$

Thus, $\varphi_0(< \theta)$ also indicates the fraction of close pairs of clusters which are roughly at the same redshift.

When comparing $\varphi_0(< \theta)$ with the actual pair count in the N -body simulations, we need to quantify what we mean by *close* along the line of sight. We compute $\varphi_0(< \theta)$ with $w(\theta)$ derived from the simulations and we choose the maximum comoving pair separation that provides a reasonable agreement between $\varphi_0(< \theta)$ and the actual count of close pairs. The comoving volume of the τ CDM model is $(2/3)^3$ smaller than the comoving volume of the Λ CDM model, but the two volumes contain the same total mass; we thus choose, for the two models, two different maximum comoving separations whose ratio is $2/3$: therefore, we have the same mass within the volumes defined by these separations. Figure 3 shows that the agreement between $\varphi_0(< \theta)$ derived from the simulations (bold lines) and the actual pair count (squares) with cluster member three-dimensional comoving separation smaller than 16 (10.7) h^{-1} Mpc for the Λ CDM (τ CDM) model is satisfactory. Dotted lines show $\varphi_0(< \theta)$ computed with the analytic model. The agreement between the simulations and the analytic model is excellent.

Figure 3 shows that the analytic model predicts that more than $\sim 70\%$ of the pairs with angular separation $\theta < 20$ arcmin are physical associations in the shallow survey $F_{\nu}^{\min} > 200$ mJy at $\nu = 143$ GHz. Because of the larger number of clusters per square degree, the fraction of pairs close in three dimensions drops to $\sim 30\%$ in the deeper survey $F_{\nu}^{\min} > 50$

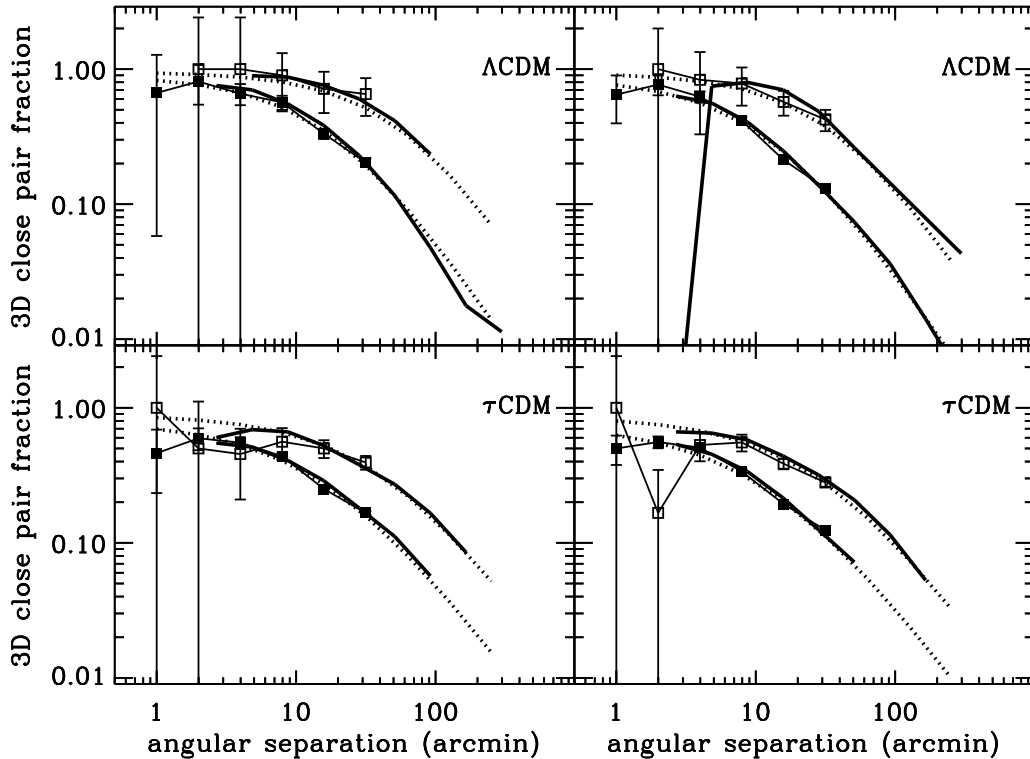


Figure 3. Fraction of cluster pairs with comoving separation < 16.0 (10.7) h^{-1} Mpc for the Λ CDM (τ CDM) model (squares). Upper (lower) curves are for $F_{\nu}^{\min} > 200$ (50) mJy. Left (right) panels are for $\nu = 143$ (353) GHz. Bold lines correspond to $\varphi_0(< \theta)$ where $w(\theta)$ is computed directly from the N -body simulations. Dotted lines are the corresponding analytic functions (equation 24). Error bars assume Poisson statistics.

mJy; this fraction is still substantial. Moscardini et al. (2002) show that, because the properties of the ICM affect the cluster mass threshold, for a fixed specific flux threshold F_{ν}^{\min} , the correlation length r_0 measured for SZ clusters is more sensitive to the ICM properties than to the cosmological parameters. According to their results, however, our estimated fractions of physically associated pairs can change by 30% at most.

The cumulative redshift distribution of the fraction of physically associated cluster pairs with angular separation in the range (θ_1, θ_2) is

$$\varphi(z, \theta_1, \theta_2) = \frac{\int_{\theta_1}^{\theta_2} \Xi(z, \theta, F_{\nu}^{\min}) \theta d\theta}{\int_{\theta_1}^{\theta_2} [\eta_0^2(F_{\nu}^{\min}) + \Xi_0(\theta, F_{\nu}^{\min})] \theta d\theta}. \quad (25)$$

Figure 4 compares the model with the simulations. The agreement is satisfactory. Shallower surveys will detect only massive clusters which form at late times. Therefore most pairs of close clusters are at moderately low redshift.

To compute the number of pairs with separation θ on the sky, consider the probability $\eta_0^2[1 + w(\theta)]d\Omega_1 d\Omega_2$ of having such a pair, where $d\Omega_i$ is the infinitesimal solid angle around each pair member and the angle between the versors pointing to $d\Omega_1$ and $d\Omega_2$ is θ . Without loss of generality, we can fix the versor of $d\Omega_1$ coincident with the z -axis and write $d\Omega_2 = d\phi_2 d\cos\theta_2 \equiv d\phi_2 d\cos\theta$. Integrating over $d\Omega_1 d\phi_2$ yields $\int d\Omega_1 d\Omega_2 = 8\pi \sin\theta d\theta$. All over the sky, the number of pairs with separation in the range $(\theta, \theta + d\theta)$ is thus $\tilde{n}_p(\theta)d\theta = 8\pi^2 \eta_0^2 [1 + w(\theta)] \sin\theta d\theta / (2 + \langle w \rangle)$, where $\langle w \rangle = \int_0^\pi \sin\theta w(\theta) d\theta$ and the relation is normalized such that it yields a total of $(4\pi\eta_0)^2/2$ pairs at any separation. In a survey with area $\Delta\Omega$, the number of pairs with angular separation in the range (θ_1, θ_2) is trivially $(\Delta\Omega/4\pi) \int_{\theta_1}^{\theta_2} \tilde{n}_p(\theta) d\theta$. We use this relation in the next section.

3.4 A survey example

To get a better idea of the sample sizes, consider a full sky survey, like the one that will be performed, for example, by the Planck surveyor, with a specific flux difference limit 100 mJy at 143 GHz. In a Λ CDM (τ CDM) model, this survey would detect ~ 5500 (17400) clusters and ~ 155 (1150) pairs with angular separation in the range 8–16 arcmin. Of these pairs,

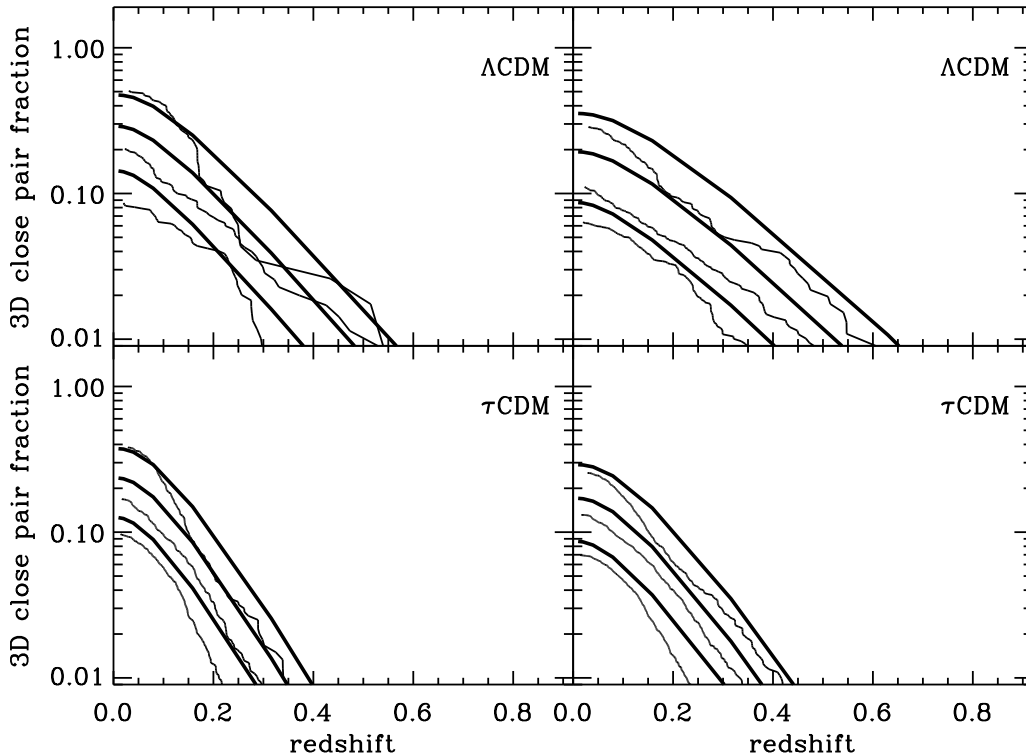


Figure 4. Cumulative redshift distribution of the fraction of cluster pairs with comoving separation < 16.0 (10.7) h^{-1} Mpc, $F_{\nu}^{\min} > 50$ mJy, and angular separation in the range (8, 16), (16, 32) and (32, 64) arcmin (top to bottom) for the Λ CDM (τ CDM) N -body models (thin lines). Left (right) panels are for $\nu = 143$ (353) GHz. Bold lines show the corresponding analytic distributions $\varphi(z, \theta_1, \theta_2)$ (equation 25).

83% (53%) are also close along the line of sight. It means that measuring the redshift of 155×2 (1150×2) clusters in close pairs would yield 128 (614) physically associated pairs and 54 (1052) “isolated” clusters. These numbers are computed with the analytic model described above. The differential redshift distributions $\bar{n}_c(z)$ of the 310 (2300) clusters and $\bar{n}_p(z)$ of the 128 (614) pairs are shown in figure 5.

Extracting the cosmology information from the cluster redshift distribution is not trivial. The redshift distribution of clusters depends on the cosmological parameters in a complicated way, through the geometry of the Universe and the cluster mass function (equation 8). The redshift distribution of pairs introduces further complications due to the cluster bias function and the non linear evolution of the dark matter correlation function (equation 19). So an estimation of the cosmological parameters with a traditional least squares fitting procedure is very cumbersome. A simpler procedure is to compare the observed distributions with those predicted by a few fiducial models. Therefore, we perform the following Monte Carlo simulation. First, by assuming a cosmological model, we use our analytical model to compute the expected number of clusters $\bar{n}_c(z)$ and pairs of clusters $\bar{n}_p(z)$ in a given redshift bin. We then generate samples of clusters and cluster pairs from Poisson distributions with mean values $\bar{n}_c(z)$ and $\bar{n}_p(z)$, respectively.

Finally we compute

$$\chi^2_{i|j} = \sum_{z \text{ bin}} \frac{(n_j - \bar{n}_i)^2}{\bar{n}_i} \quad (26)$$

where the sum is over the redshift bins, the indices i and j refer to the cosmological model (e.g., Λ CDM or τ CDM), n_j is the variable drawn from model j and \bar{n}_i is the expected mean value in model i .

The lower panels of figure 5 show the distribution of the χ^2 for 10^4 Monte Carlo realizations drawn from the redshift distributions shown in the upper panels. Each random sample (either of clusters or pairs of clusters) drawn from a model j is a point on the plane $\chi^2_{\tau|j} - \chi^2_{\Lambda|j}$ in figure 5. Both the cluster and pair samples would give significant large χ^2 when compared to the wrong cosmological model.

3.5 Sensitivity on the biasing relation

The predicted number of physically associated cluster pairs depends on the assumed biasing relation between the cluster and the mass distribution. In the previous sections, we have assumed a time and scale dependent bias factor (equation 22). To

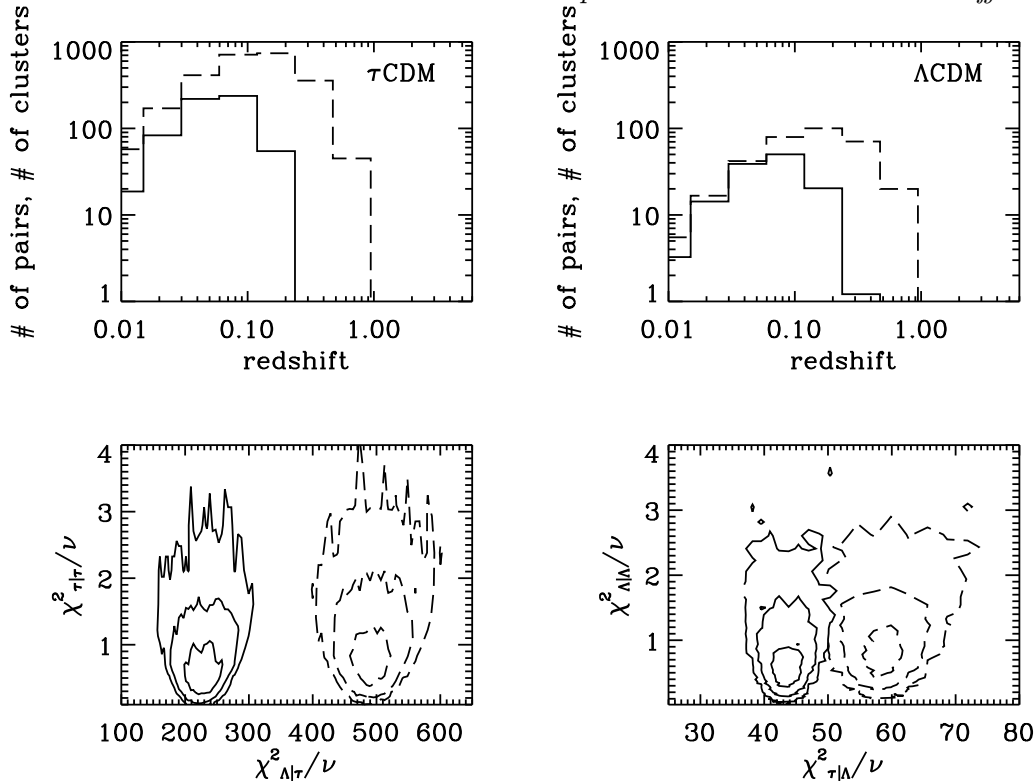


Figure 5. Upper panels: differential redshift distribution $n_p(z)$ of physically associated pairs of clusters with angular separation in the range 8–16 arcmin for a full sky survey with $F_\nu^{\min} = 100$ mJy and $\nu = 143$ GHz (solid histograms); differential redshift distribution $n_c(z)$ of all the clusters in pairs with angular separation in the range 8–16 arcmin, irrespective of their physical association, in the same survey (dashed histograms). Lower panels: probability density of the reduced χ^2 of Monte Carlo realizations drawn from the τ CDM model (left panel) and the Λ CDM model (right panel) computed with respect to each model. Solid (dashed) contours are for the pair (cluster) samples. Contour levels are (0.61,0.13,0.01) times the maximum probability density. They roughly correspond to the 68%, 95% and 99% confidence levels.

investigate how sensitive the fraction of pairs is on this assumption, we consider two extreme models: a scale independent and a time independent bias factors. Namely,

$$b_{\text{no-}r}(z, F_\nu^{\min}) = b_{\text{ST,eff}}(z, F_\nu^{\min}) \quad (27)$$

and

$$b_{\text{no-}z}(r, F_\nu^{\min}) = b_{\text{ST,eff}}(0, F_\nu^{\min}) [1 + b_{\text{ST,eff}}(0, F_\nu^{\min}) \sigma(r, 0)]^{0.35} . \quad (28)$$

Figure 6 shows our fiducial biasing relation $b_{\text{eff}}(r, z, F_\nu^{\min})$; in this figure, the bottom lines of the Λ CDM and τ CDM models show the time independent bias factor $b_{\text{no-}z}(r, F_\nu^{\min})$. Figure 7 show the scale independent bias factor $b_{\text{no-}r}(z, F_\nu^{\min})$.

Figure 8 shows that neglecting the scale dependence considerably suppresses the angular correlation function (dotted lines). Because clusters form at relatively low redshift, neglecting the time dependence is less dramatic (dashed lines): in fact, the number of physically associated pairs is substantially underestimated only at $z > 0.2$ (bottom panels).

To quantify how significant the difference between these biasing relations is, we proceed as in section 3.4. We draw 10^4 Monte Carlo realizations from the redshift distributions of the physically associated cluster pairs shown in the bottom right panel of figure 8. We compute the variable χ_{ij}^2 (equation 26), where now i and j stay for our fiducial (equation 22), scale independent (equation 27) or time independent (equation 28) biasing relations.

Our results are shown in figure 9. The difference between our fiducial model and the scale independent model generates large χ^2 values when compared to each other (top panels). The difference between our fiducial model and the time independent model, although substantially smaller, is still well measurable (bottom panels).

4 DISCUSSION AND CONCLUSION

One of the main purposes of SZ cluster surveys is to constrain the cosmological model with the cluster redshift distribution. In fact, the redshift distribution of SZ selected clusters depends on the density parameter Ω_0 , the mass power spectrum, and the physical properties of the ICM. Therefore one hopes that catalogues of SZ clusters can constrain the cosmological models

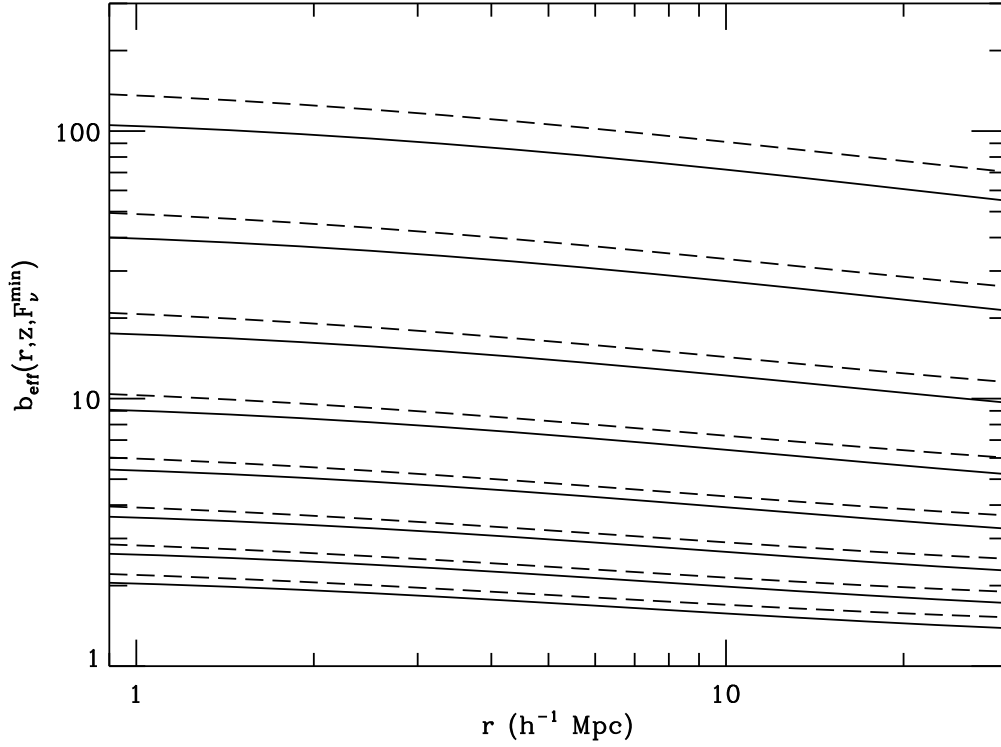


Figure 6. Effective bias (equation 22) of SZ selected clusters in a survey with $F_{\nu}^{\min} = 50$ mJy and $\nu = 143$ GHz. Solid (dashed) lines are for the Λ CDM (τ CDM) model. Curves are for $z = 0.01, 0.02, 0.06, 0.14, 0.34, 0.82, 2.0, 4.8$ (bottom to top).

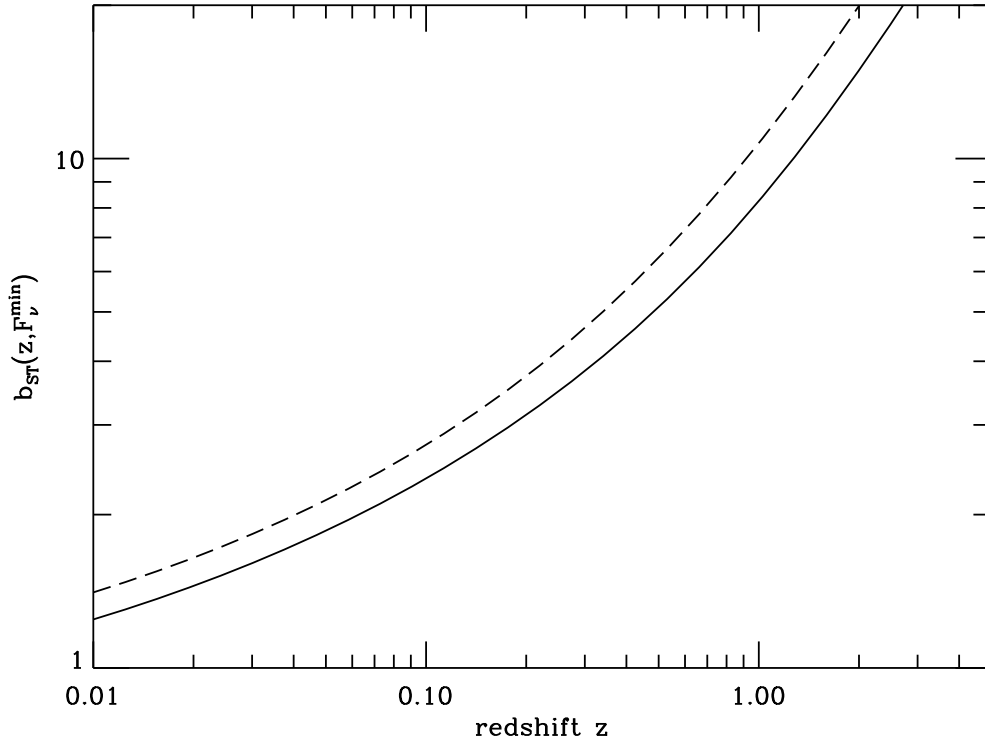


Figure 7. Effective scale independent bias (equation 27) of SZ selected clusters in a survey with $F_{\nu}^{\min} = 50$ mJy and $\nu = 143$ GHz. Solid (dashed) line is for the Λ CDM (τ CDM) model.

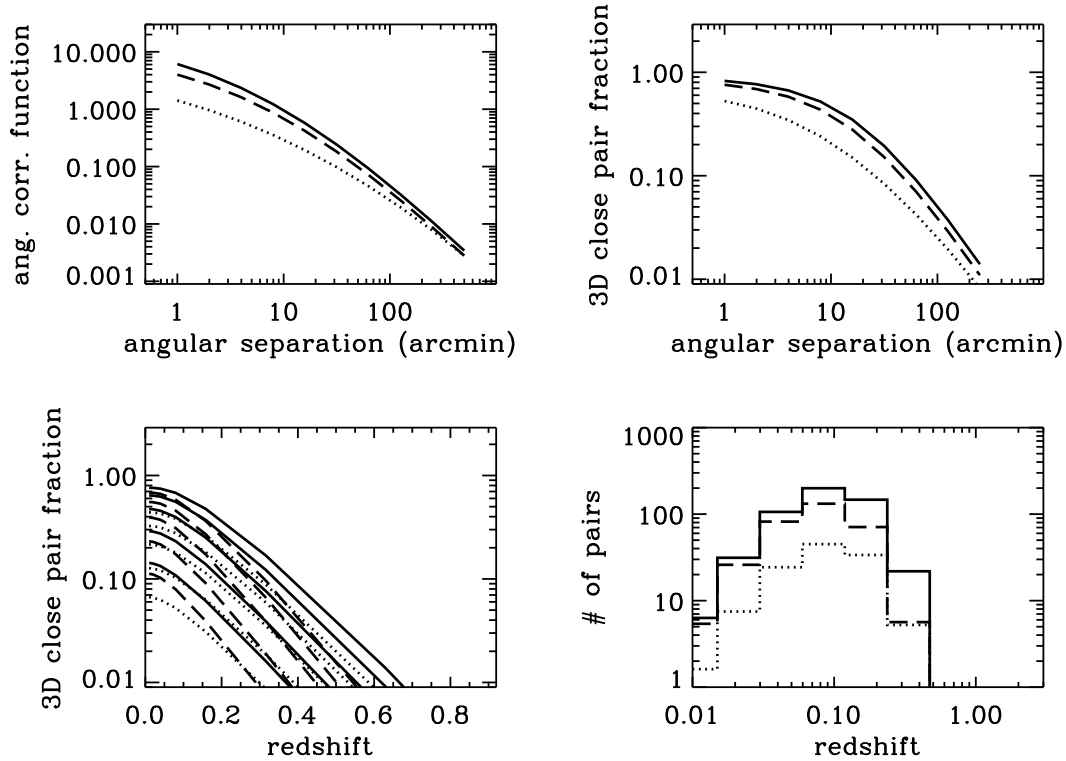


Figure 8. Sensitivity of our results on the biasing relation in the Λ CDM model for a survey with $F_{\nu}^{\min} = 50$ mJy and $\nu = 143$ GHz. Solid, dashed and dotted lines refer to our fiducial (equation 22), time independent (equation 28) and scale independent (equation 27) biasing relations, respectively. The bottom right panel shows the redshift distribution of physically associated cluster pairs with angular separation in the range 8-16 arcmin in a full sky survey.

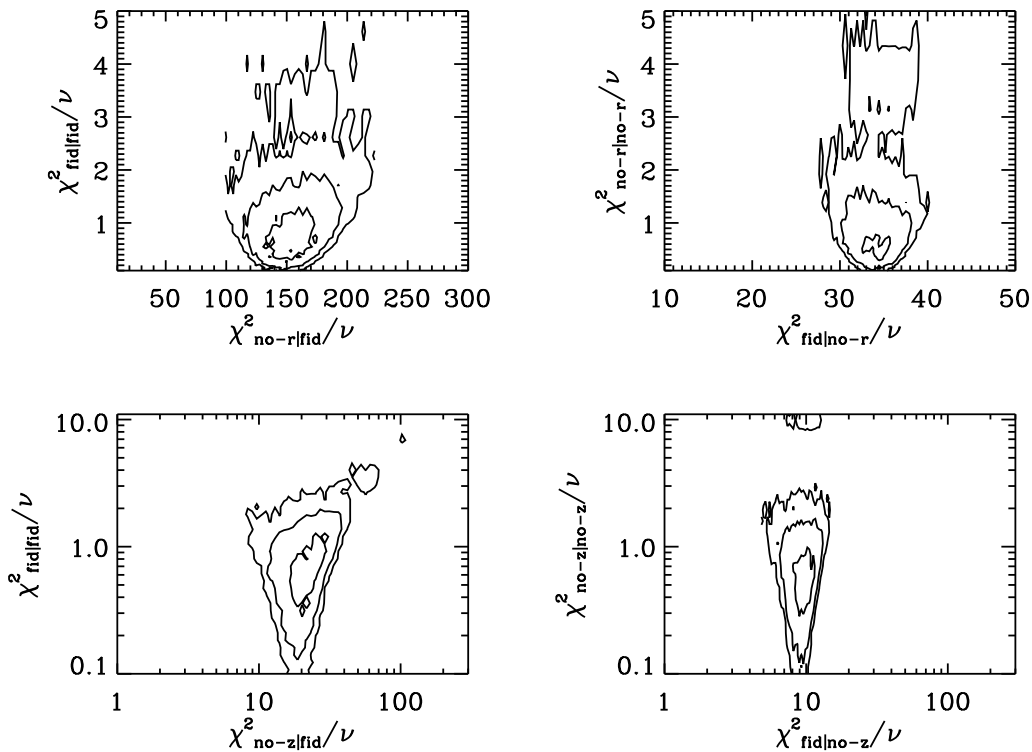


Figure 9. Values of the χ^2 corresponding to the bottom right panel of figure 8. See text for more information. Contour levels are (0.61,0.13,0.01) times the maximum probability density. They roughly correspond to the 68%, 95% and 99% confidence levels.

despite the degeneracies between some parameters such as the normalization of the power spectrum σ_8 and Ω_0 (Barbosa et al. 1996; Kneissl et al. 2001; Holder, Haiman & Mohr 2001; Benson, Reichardt & Kamionkowski 2002).

However, for the very same reason why SZ cluster surveys are so attractive, their catalogues will not have any accurate information on the cluster distances, although the morphology of the cluster can provide a rough estimate of its redshift (Diego et al. 2002). The redshift distribution of clusters can be determined with follow up optical observations, CO line measurement in galaxy cluster members, or high resolution X-ray spectroscopy (e.g. Bleeker & Mendez 2002). The number of objects in SZ cluster surveys depends on the sky coverage, instrumental sensitivity, and observational bands. In an all sky surveys, this number can be of order several thousands. Of course, only the redshifts of a subsample of these clusters is sufficient to provide a robust estimate of the redshift distribution. How should one choose this cluster subsample? We suggest to measure the redshift of clusters in close pairs. Because the probability that clusters close on the sky are also close along the line of sight is substantial, this strategy will provide, at the same time, the redshift distribution of clusters and a catalogue of superclusters.

To show that the compilation of a catalogue of superclusters from SZ cluster surveys is indeed feasible, we have computed the angular correlation function of SZ selected clusters for two cosmological models. We have then computed how many cluster pairs, close on the sky, are also close along the line of sight. For example, for clusters with specific flux difference larger than 200 mJy at 143 GHz in a Λ CDM model, 70% of the pairs with angular separations smaller than 20 arcmin are physical associations. Because an SZ supercluster catalogue will contain superclusters at any redshifts thanks to the redshift independence of the SZ effect, the catalogue will be of great relevance for follow up studies of the evolution of galaxy and cosmic structures in high density regions. Moreover, from the redshift distribution of physically associated cluster pairs, we can extract information on the biasing relation between the cluster and the mass distribution.

To compute the number of detectable clusters, we have used the point source approximation, where the survey can detect the total cluster radio flux, but it cannot resolve the cluster structure. This approximation is thus independent of the cluster profile. It is realistic for poor resolution surveys (for example the Planck surveyor will perform a survey with a beam FWHM of 8 arcmin at 143 GHz), but of course unrealistic for high resolution bolometric or interferometric ground-based surveys. However, resolving the clusters has the net effect of increasing the mass threshold and thus decreasing the number of detected sources (Bartlett 2000). In other words, resolving the cluster structure is similar to considering our results for shallower surveys: the cluster minimum mass is larger and the fraction of physically associated pairs increases.

ACKNOWLEDGMENTS

We thank Lauro Moscardini for fruitful discussions. The Hubble Volume N -body simulations used in this paper were carried out by the Virgo Supercomputing Consortium using computers based at the Computing Centre of the Max-Planck Society in Garching and at the Edinburgh parallel Computing Centre. The data are publicly available at <http://www.mpa-garching.mpg.de/NumCos>. This research was partially supported by the NATO Collaborative Linkage Grant PST.CLG.976902, the Italian MIUR grant COFIN2001028932 “Clusters and groups of galaxies: the interplay of dark and baryonic matter”, the EC RTN network “The Physics of the Intergalactic Medium”, and a grant from the G.I.F., the German Israeli Foundation for Scientific Research and Development. AN is supported by a grant from the Israeli Science Foundation and the Technion Fund for the Promotion of Research. We acknowledge use of the abstract server at the NASA’s Astrophysics Data System and the archive of the astro-ph preprint server.

REFERENCES

- Aghanim N., Gorski K. M., Puget J.-L., 2001, *A&A*, 374, 1
- Allen S. W., Schmidt R. W., Fabian A. C., 2001, *MNRAS*, 328, L37
- Bahcall N. A., Gramann M., Cen R., 1994, *ApJ*, 436, 23
- Bahcall N. A., Soneira R. M., 1984, *ApJ*, 277, 27
- Barbosa D., Bartlett J. G., Blanchard A., Oukbir J., 1996, *A&A*, 314, 13
- Bardelli S., Zucca E., Baldi A., 2001, *MNRAS*, 320, 387
- Bartlett J. G., 2000, *A&A*, submitted (astro-ph/0001267)
- Bartlett J. G., 2001, in *Tracing cosmic evolution with galaxy clusters (Sesto Pusteria 3-6 July 2001)*, ASP Conference Series in press (astro-ph/0111211)
- Bartlett J. G., Silk J., 1994, *ApJ*, 423, 12
- Basilakos S., Plionis M., Rowan-Robinson M., 2001, *MNRAS*, 323, 47
- Benson A. J., Reichardt C., Kamionkowski M., 2002, *MNRAS*, 331, 71
- Bleeker J., Mendez M. 2002, astro-ph/0207283
- Bryan G. L., Norman M. L. 1998, *ApJ*, 495, 80
- Carlstrom J. E., 2002, *ARA&A*, 40, in press

- Colberg J. M., White, S. D. M., MacFarland T. J., Jenkins A., Pearce F. R., Frenk C. S., Thomas P. A., Couchman H. M. P., 2000a, *MNRAS*, 313, 229
- Colberg J. M., et al. 2000b, *MNRAS*, 319, 209
- Cole S., Kaiser N., 1988, *MNRAS*, 233, 637
- da Silva A. C., Barbosa D., Liddle A. R., Thomas P. A., 2000, *MNRAS*, 317, 37
- Diaferio A., Sunyaev R. A., Nusser A., 2000, *ApJ*, 533, L71
- Diego J. M., Mohr J., Silk J., Bryan G. 2002, *MNRAS*, submitted
- Einasto M., Einasto J., Tago E., Müller V., Andernach H., 2001, *AJ*, 122, 2222
- Ettori S., Fabian A. C., 1999, *MNRAS*, 305, 834
- Evrard A. E., et al., 2002, *ApJ*, 573, 7
- Finoguenov A., Reiprich T. H., Böhringer H., 2001, *A&A*, 368, 749
- Frenk C. S., et al., 2000, *astro-ph/0007362*
- Haiman Z., Mohr J. J., Holder G. P., 2001, *ApJ*, 553, 545
- Hamana T., Yoshida N., Suto Y., Evrard A. E., 2001, *ApJ*, 561, L143
- Hashimoto Y., Hasinger G., Arnaud M., Rosati P., Miyaji T., 2002, *A&A*, 381, 841
- Holder G. P., Carlstrom J. E., 2001, *ApJ*, 558, 515
- Holder G. P., Haiman Z., Mohr J. J., 2001, *ApJ*, 560, L111
- Jenkins A., Frenk C. S., White S. D. M., Colberg J. M., Cole S., Evrard A. E., Couchman H. M. P., Yoshida N., 2001, *MNRAS*, 321, 372
- Kerscher M., 1998, *A&A*, 336, 29
- Kitayama T., Suto Y., 1996, *ApJ*, 469, 480
- Kneissl R., Jones M. E., Saunders R., Eke V. R., Lasenby A. N., Grainge K., Cotter G., 2001, *MNRAS*, 328, 783
- Kolokotronis V., Plionis M., Basilakos S., 2002, *MNRAS*, 331, 1020
- Komatsu E., Kitayama T., 1999, *ApJ*, 526, L1
- Korolev V. A., Sunyaev R. A., Yakubsev L. A., 1986, *Sov. Astron. Lett.* 12, 141
- Lo K. Y., Chiueh T. H., Martin R. N., Ng K.-W., Liang H., Pen U.-I., Ma Ch.-P., 2002, in *New Cosmological Data and the Values of the Fundamental Parameters*, IAU Symposium 201, edited by A. N. Lasenby and A. Wilkinson, in press
- Matarrese S., Coles P., Lucchin F., Moscardini L., 1997, *MNRAS*, 286, 115
- Mather J. C., Fixsen D. J., Shafer R. A., Mosier C., Wilkinson D. T., 1999, *ApJ*, 512, 511
- Mathiesen B. F., Evrard A. E., 2001, *ApJ*, 546, 100
- Moscardini L., Matarrese S., Lucchin F., Rosati P. 2000, *MNRAS*, 316, 283
- Moscardini L., Bartelmann M., Matarrese S., Andreani P., 2002, *MNRAS*, in press
- Nakamura T. T., Suto Y., 1997, *Progress of Theoretical Physics*, 97, 49
- Oort J. H., 1983, *ARA&A*, 21, 373
- Osmer P. S., 1981, *ApJ*, 247, 762
- Peacock J. A., Dodds S. J., 1996, *MNRAS*, 280, L19
- Peel A., Knox L. 2002, *astro-ph/0205438*
- Plionis M., Basilakos S., 2002, *MNRAS*, 329, L47
- Porciani C., 1997, *MNRAS*, 290, 639
- Postman M., Lauer T. R., Oegerle W., Donahue M. 2002, *astro-ph/0205513*
- Rines K., Mahdavi A., Geller M. J., Diaferio A., Mohr J. J., Wegner G., 2001, *ApJ*, 555, 558
- Scaramella R., Cen R., Ostriker J. P., 1993, *ApJ*, 416, 399
- Seljak U., Burwell J., Pen U., 2000, *astro-ph/0001120*
- Sheth R. K., Diaferio A., 2001, *MNRAS*, 322, 901
- Sheth R. K., Tormen G., 1999, *MNRAS*, 308, 119
- Small T. A., Ma C.-P., Sargent W. L. W., Hamilton D., 1998, *ApJ*, 492, 45
- Springel V., White M., Hernquist L., 2001, *ApJ*, 549, 681
- Sunyaev R. A., Zel'dovich Ya. B., 1980, *ARA&A*, 18, 537 (SZ)
- Voit G. M., 2000, *ApJ*, 543, 113
- Weinberg S., 1972, *Gravitation and Cosmology: Principles and Applications of the General Theory of Relativity*, John Wiley & Sons, New York
- West M. J., 1989, *ApJ*, 347, 610
- West M. J., 1991, *ApJ*, 379, 19
- Yoshida N., et al. 2001, *MNRAS*, 325, 803
- Yoshikawa K., Taruya A., Jing Y. P., Suto Y., 2001, *ApJ*, 558, 520
- Zhang P., Pen U., Wang B., 2002, *astro-ph/0201375*
- Zucca E., Zamorani G., Scaramella R., Vettolani G., 1993, *ApJ*, 407, 470